JVST A
Journal of Vacuum Science & Technology A

ARTICLE

avs.scitation.org/journal/jva

Thermal atomic layer etching of amorphous and crystalline Al_2O_3 films

Cite as: J. Vac. Sci. Technol. A 39, 042602 (2021); doi: 10.1116/6.0000995
Submitted: 21 February 2021 · Accepted: 17 May 2021 ·
Published Online: 9 June 2021

Jessica A. Murdzek,[1] Adarsh Rajashekhar,[2] Raghuveer S. Makala,[2] and Steven M. George[1]

AFFILIATIONS

[1]Department of Chemistry, University of Colorado, Boulder, Colorado 80309
[2]Thin Films and New Materials Team, Silicon Technology and Manufacturing, Western Digital Corporation, 951 SanDisk Dr., Milpitas, California 95035

Note: This paper is part of the 2022 Special Topic Collection on Atomic Layer Etching (ALE).

ABSTRACT

Thermal atomic layer etching (ALE) can be achieved with sequential, self-limiting surface reactions. One mechanism for thermal ALE is based on fluorination and ligand-exchange reactions. For metal oxide ALE, fluorination converts the metal oxide to a metal fluoride. The ligand-exchange reaction then removes the metal fluoride by forming volatile products. Previous studies have demonstrated the thermal ALE of amorphous Al_2O_3 films. However, no previous investigations have explored the differences between the thermal ALE of amorphous and crystalline Al_2O_3 films. This study explored the thermal ALE of amorphous and crystalline Al_2O_3 films. HF, SF_4, or XeF_2 were used as the fluorination reactants. Trimethylaluminum (TMA) or dimethylaluminum chloride (DMAC) were used as the metal precursors for ligand-exchange. Spectroscopic ellipsometry measurements revealed that the amorphous Al_2O_3 films had much higher etch rates than the crystalline Al_2O_3 films. When using HF and TMA at 300 °C, the amorphous Al_2O_3 film was removed at an etch rate of 0.78 Å/cycle. For the crystalline Al_2O_3 film, an etch rate of 0.06 Å/cycle was initially observed prior to the stoppage of etching after removing about 10 Å of the film. Thermal ALE with HF and DMAC resulted in similar results. Etch rates of 0.60 and 0.03 Å/cycle were measured for amorphous and crystalline Al_2O_3 films at 300 °C, respectively. Other fluorination agents, such as SF_4 or XeF_2, were also used together with TMA or DMAC for Al_2O_3 ALE. These reactants for fluorination and ligand-exchange were able to etch amorphous Al_2O_3 films at 300 °C. However, they were unable to etch crystalline Al_2O_3 film at 300 °C beyond the initial 10–20 Å surface layer. The investigations also examined the effect of annealing temperature on the etch rate per cycle using HF and TMA as the reactants at 300 °C. Amorphous Al_2O_3 films were etched at approximately the same etch rate of 0.78 Å/cycle until the crystallization of amorphous Al_2O_3 films at $\geq$ 880 °C. The differences between amorphous and crystalline Al_2O_3 thermal ALE could be used to obtain selective thermal ALE of amorphous Al_2O_3 in the presence of crystalline Al_2O_3.

I. INTRODUCTION

ALE is a technique that can remove thin films with Ångstrom-level precision using sequential, self-limiting surface reactions.[1] There are two major types of ALE: plasma[1,2] and thermal.[3,4] Plasma ALE is an anisotropic etching technique based on surface modification followed by an exposure of energetic ions or neutrals that remove material.[1,2,5] Thermal ALE is an isotropic etching technique and is often viewed as the opposite of atomic layer deposition (ALD).[3,6,7] Similar to ALD, thermal ALE utilizes sequential exposures of gaseous reactants with inert gas purging in between the reactant exposures.[3,4]

A common thermal ALE mechanism is based on fluorination and ligand-exchange reactions to achieve etching.[3,4,8] For metal oxides, the fluorination reaction converts a thin surface layer of the metal oxide into a metal fluoride.[9,10] The ligand-exchange reaction then creates a volatile metal product that results in the removal of the surface metal fluoride layer.[11] The ligand-exchange step involves a metal precursor accepting a fluoride ligand while donating one of its ligands to the metal fluoride surface. Etching occurs when this ligand-exchange creates stable, volatile products.[11]

Thermal ALE using the fluorination and ligand-exchange pathway has been used to etch many metal oxides, such as Al_2O_3,[4,9,12,13] ZrO_2,[14] HfO_2,[14,15] and Ga_2O_3.[16] The same fluorination and ligand-exchange process has also successfully etched metal nitrides such as AlN (Ref. 17) and GaN.[18] Other mechanisms for

thermal ALE utilize conversion reactions.[19] During conversion reactions, the surface of the thin film of interest is converted into a new material.[19] Conversion reactions have been used to etch SiO_2 (Ref. 20) and ZnO.[21] In addition, thermal ALE of W,[22] Si,[23] Si_3N_4,[24] and SiGe (Ref. 25) can be accomplished via oxidation and conversion reactions.

Thermal ALE of amorphous Al_2O_3 is typically performed using fluorination and ligand-exchange reactions. Previous studies have used HF for fluorination,[4,9,12,13] and $Sn(acac)_2$,[4,12] trimethylaluminum (TMA),[13] or dimethylaluminum chloride (DMAC)[14,26,27] for ligand-exchange. The process for etching Al_2O_3 with HF and TMA is shown in Fig. 1.[13] There have been no reports of thermal ALE for crystalline Al_2O_3. However, other crystalline materials, such as AlN and GaN, have been etched with thermal ALE.[17,18]

One previous study examined the difference in thermal ALE between crystalline and amorphous HfO_2, ZrO_2, and $HfZrO_4$.[28] Amorphous HfO_2, ZrO_2, and $HfZrO_4$ were observed to etch more rapidly than their corresponding crystalline counterparts using HF and $TiCl_4$ as the reactants at 250 °C.[28] The differences were not as great using HF and DMAC as the reactants at 250 °C. In particular, ZrO_2 showed very little difference between the amorphous and crystalline forms.[28] A similar study comparing crystalline and amorphous Al_2O_3 will be presented in this paper.

Al_2O_3 has many different crystalline structures.[29] Amorphous Al_2O_3 is a glassy, disordered state of Al_2O_3 that can be formed by either physical vapor deposition (PVD) or atomic layer deposition (ALD).[30,31] Upon annealing to temperatures >800 °C, amorphous Al_2O_3 films deposited using electron beam evaporation crystallized into gamma-Al_2O_3 and other phases such as delta-Al_2O_3.[32] The annealing of Al_2O_3 ALD films also results in a mixture of crystalline phases including gamma-Al_2O_3 upon crystallization.[33–35] As the Al_2O_3 film is annealed to higher temperatures, the crystalline structure evolves and finally reaches the alpha-Al_2O_3 crystalline phase at temperatures >1100 °C.[32,35] The crystalline Al_2O_3 films used in this study were prepared by annealing in the range of 800–1000 °C and displayed x-ray diffraction peaks that were consistent with gamma-Al_2O_3 and delta-Al_2O_3.

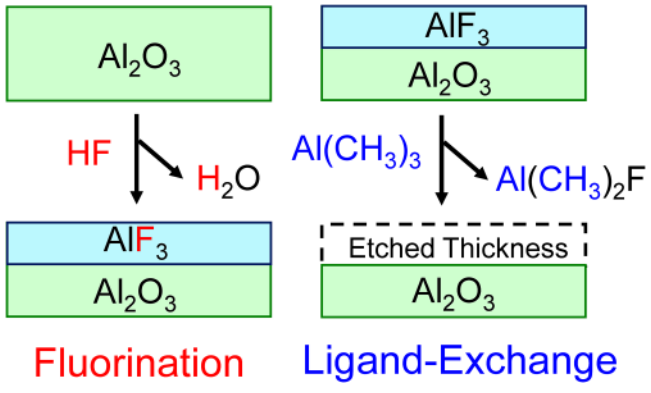

FIG. 1. Schematic for thermal Al_2O_3 ALE using HF for fluorination and TMA for ligand-exchange.

The etching of crystalline Al_2O_3 films is important because obtaining ultrathin films of crystalline metal oxides can be difficult. The crystallization temperature typically increases as the Al_2O_3 film thickness decreases.[34,36] For example, for a 60 s annealing process, an 8 nm Al_2O_3 ALD film could be crystallized at 850 °C as determined by x-ray diffraction analysis.[34] In contrast, for the same 60 s annealing process, a 5 nm Al_2O_3 ALD film required 900 °C to crystallize, and a 3.5 nm Al_2O_3 ALD film required 1000 °C to crystallize.[34] Crystallization temperatures that increased for thinner Al_2O_3 film thicknesses were also observed using differential scanning calorimetry studies.[36]

The trend that thinner films require higher temperatures to crystallize is well established for other metal oxide films.[37–40] The increase in crystallization temperature as the film decreases in thickness is explained by the increase in surface-to-volume ratio.[38,40] Al_2O_3 ALE could avoid the high thermal budget necessary for crystallizing ultrathin Al_2O_3 films.[32,34,36] A thicker Al_2O_3 film could be grown using Al_2O_3 ALD and then annealed for crystallization. Subsequently, the thicker crystalline Al_2O_3 film could be etched back to the desired ultrathin thickness.[8,28]

Differences between amorphous and crystalline thermal ALE etch rates are also important for selective ALE. Selectivity is achieved when two materials have different etch rates under the same conditions.[14] Selectivity could be observed for the crystalline and amorphous forms of the same material if the two have different etch rates. Crystalline thin films of HfO_2, ZrO_2, and $HfZrO_4$ have been shown to etch more slowly than their corresponding amorphous thin films.[28] A similar trend may be observed for Al_2O_3 ALE. A possible application would be the selective etching of ultrathin Al_2O_3 films. For example, a low temperature anneal of Al_2O_3 films of various thicknesses would only crystallize the thicker films. The thinner amorphous Al_2O_3 films that did not crystallize would then be etched via thermal Al_2O_3 ALE.

For this study, fluorination and ligand-exchange reactions were used to etch amorphous and crystalline Al_2O_3 films. The fluorination reactants were HF, SF_4, and XeF_2. The ligand-exchange reactants were TMA and DMAC. The experiments were all conducted at 300 °C. Film thickness measurements were performed versus number of thermal ALE cycles using *ex situ* spectroscopic ellipsometry (SE). Plots of film thickness versus number of ALE cycles were used to determine the etch rates.

II. EXPERIMENT

The thermal ALE experiments were performed in a viscous flow reactor.[28,41] The reaction temperatures were maintained by a proportional-integral-derivative (PID) temperature controller (2604, Eurotherm). A constant flow of ultrahigh purity (99.999%) N_2 gas was employed as the carrier and purge gas. Mass flow controllers (Type 1179A, MKS) regulated the nitrogen gas flow. A mechanical pump (Pascal 2015SD, Alcatel) was attached to the back of the reactor. The reactor pressure with flowing N_2 carrier gas was ~1 Torr. The reactor pressure was measured by a capacitance manometer (Baratron 121A, MKS).

The fluorination reactions used either HF-pyridine solution (70 wt. % HF, Sigma-Aldrich), SF_4 (>98.5%, SynQuest Laboratories), or XeF_2 (99.5%, Strem Chemicals). All fluorination

agents were maintained at room temperature. The HF-pyridine solution was contained in a gold-plated stainless steel bubbler to prevent corrosion. The pressure transients of HF from the HF-pyridine source were adjusted to ~90 mTorr using a metering valve (SS-4BMG, Swagelok). The XeF_2 pressure transients were ~10 mTorr without a metering valve. The SF_4 pressure was metered to ~200 mTorr. The ligand-exchange precursors were TMA (97%, Sigma-Aldrich) and DMAC (97%, Sigma-Aldrich). Both ligand-exchange reactants were held at room temperature. Metering valves were used to maintain pressure transients of ~40 mTorr for both TMA and DMAC.

Crystalline and amorphous aluminum oxide thin films on native oxide silicon wafer coupons were used for these studies. Some of the Al_2O_3 ALD films were grown using methyl or chloride-based aluminum precursors and water at temperatures in the range of 200–250 °C. An SSI Solaris 200 Rapid Thermal Processing system was used for crystallizing the amorphous Al_2O_3 films. The first set of crystalline Al_2O_3 films were obtained by subjecting the Al_2O_3 ALD films to rapid thermal annealing at 1000 °C. These Al_2O_3 films had a thickness of approximately 5 nm.

The second set of samples consisted of Al_2O_3 ALD films deposited using TMA and H_2O at 200 °C. The growth of these Al_2O_3 ALD films was performed in the same reactor that was employed for the ALE studies. These Al_2O_3 ALD films were then thermally annealed at various temperatures (400, 600, 800, and 1000 °C) in an N_2 ambient for 60 s. The thickness of these Al_2O_3 ALD films was approximately 17 nm.

Grazing incidence x-ray diffraction (GI-XRD) scans were recorded using an x-ray diffractometer (Bede D1, Jordan Valley Semiconductors) with radiation from the Cu Kα line at λ = 1.540 Å. The x-ray tube filament voltage was 40 kV and current was 35 mA. The incident angle was 0.3°. GI-XRD scans for these samples are shown in Fig. 2. Only the Al_2O_3 ALD film annealed at 1000 °C displayed a diffraction peak. The diffraction peak at 67° is consistent with the gamma-Al_2O_3 or delta-Al_2O_3 structure.[32,34,42]

The third set of samples were grown using the same method as the first set of samples except that the films were annealed to 800, 840, 880, 920, 960, and 1000 °C using a rapid thermal anneal process in an N_2 ambient for 60 s. All the samples used in this study were analyzed with XRD to determine film structure and x-ray reflectivity (XRR) to measure the film densities. The XRR measurements were recorded using the same diffractometer and parameters as described for the GI-XRD scans. The XRR scan range was 500–6000 arc sec and recorded with a step size of 10 arc sec.

The film densities derived from the XRR scans are displayed in Fig. 3. The initial Al_2O_3 ALD films have densities around 3.0 g/cm^3 as expected for Al_2O_3 ALD films.[43] The films that obtain crystallinity after annealing have densities around 3.63 g/cm^3. This density is consistent with a number of Al_2O_3 polymorphs including gamma-Al_2O_3 or delta-Al_2O_3.[29] These crystalline Al_2O_3 films are not as dense as alpha-Al_2O_3 which has a density of 3.99 g/cm^3.[29]

The silicon wafers with the Al_2O_3 thin films were cut into coupons with dimensions of 2 × 2 cm^2. For each experiment, multiple samples were placed in the reactor. Running multiple samples concurrently allowed for direct comparisons between amorphous and crystalline Al_2O_3 films.

The ALE experiments were performed with a reaction sequence of x-30-2-30. This sequence signifies a fluorination reactant exposure of x seconds, then a 30 s N_2 purge, a metal precursor exposure of 2 s, and then another 30 s N_2 purge. The metal precursor exposure of 2 s was determined from previous studies of Al_2O_3 ALE.[13,14,26] Experiments using HF or SF_4 as the fluorination reactant had a reaction sequence of 1-30-2-30. When XeF_2 was used as the fluorination reactant, the reaction sequence was 3-30-2-30.

The film thicknesses were measured using *ex situ* spectroscopic ellipsometry (SE) measurements. A spectroscopic ellipsometer (M-2000, J. A. Woollam) measured Ψ and Δ from 240 to

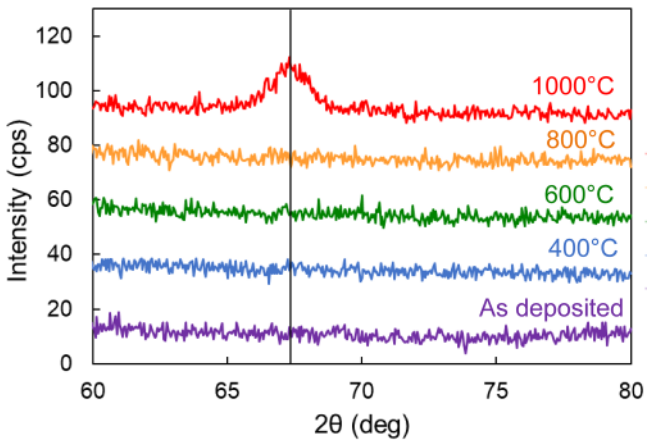

FIG. 2. GI-XRD scans for the as-deposited Al_2O_3 film, and Al_2O_3 films annealed to 400, 600, 800, and 1000 °C. The prominent peak at 67° is expected for gamma-Al_2O_3 or delta-Al_2O_3.

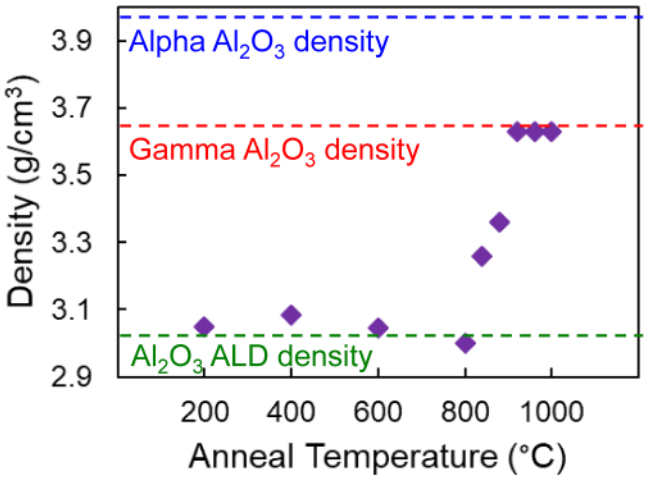

FIG. 3. Al_2O_3 film density vs anneal temperature determined by XRR analysis. Densities for Al_2O_3 ALD, gamma-Al_2O_3, and alpha-Al_2O_3 are shown for comparison.

1000 nm with an incidence angle of 70°. The CompleteEASE software was used to model the data to determine the film thickness and the optical constants, n (refractive index) and k (extinction coefficient). The etch rate was determined using film thickness measurements versus number of ALE cycles.

The precision of the SE measurements of film thickness was within ±0.05 Å. A Cauchy model was used for all the Al_2O_3 thin films. The etch rates obtained from individual ALE experiments were accurate to ±0.03 Å/cycle. The reproducibility of the etch rates as determined from repeated experiments under the same conditions was ±0.05 Å/cycle.

Atomic force microscopy (AFM) was utilized to evaluate the surface of the amorphous and crystalline Al_2O_3 films before and after ALE. These AFM measurements were performed with a Park NX10 AFM instrument using a noncontact mode. The scan rate was 0.4 Hz with an Olympus microcantilever probe (OMCL-AC160TS).

III. RESULTS AND DISCUSSION

A. Al_2O_3 etching with HF and TMA or DMAC for ligand-exchange

The etch rates were significantly different for the amorphous and crystalline Al_2O_3 samples. The initial experiment compared the first set of samples comprised of the amorphous Al_2O_3 ALD films and the crystalline Al_2O_3 films annealed to 1000 °C. The Al_2O_3 ALE results for these samples using HF and TMA as the reactants at 300 °C are shown in Fig. 4. The etch rate for the amorphous Al_2O_3 film is 0.78 Å/cycle. This etch rate is comparable with earlier measurements for the ALE of amorphous Al_2O_3 ALD films using HF and TMA at 300 °C.[13] In comparison, the etch rate for the crystalline Al_2O_3 is 0.06 Å/cycle only for the first 10 Å of the film thickness. No further etching occurs after removal of the top surface layer. This behavior may occur if the top surface layer is easier to fluorinate and remove than the bulk crystalline Al_2O_3 film.

AFM images compared the surface roughness before and after Al_2O_3 ALE. Figure 5(a) shows an AFM line scan for an initial amorphous Al_2O_3 film. The initial root mean square (RMS) surface roughness was 0.148 nm. Figure 5(b) displays an AFM line scan after Al_2O_3 ALE using HF and TMA at 300 °C removed 5.2 nm of the amorphous Al_2O_3 film. The RMS surface roughness after this etching was marginally smaller at 0.135 nm. Surface smoothing of amorphous Al_2O_3 films has been observed earlier after Al_2O_3 ALE using either HF and TMA as the reactants[21] or HF and $Sn(acac)_2$ as the reactants.[4]

Figure 6(a) shows an AFM line scan for an initial crystalline Al_2O_3 film. The initial RMS surface roughness was 0.107 nm. Figure 6(b) displays an AFM line scan after Al_2O_3 ALE using HF and TMA at 300 °C removed 0.5 nm of the crystalline Al_2O_3 film. The RMS surface roughness was slightly reduced after this etching to 0.085 nm. The Al_2O_3 ALE was able to smooth the crystalline Al_2O_3 surface. There was no evidence that the crystalline structure

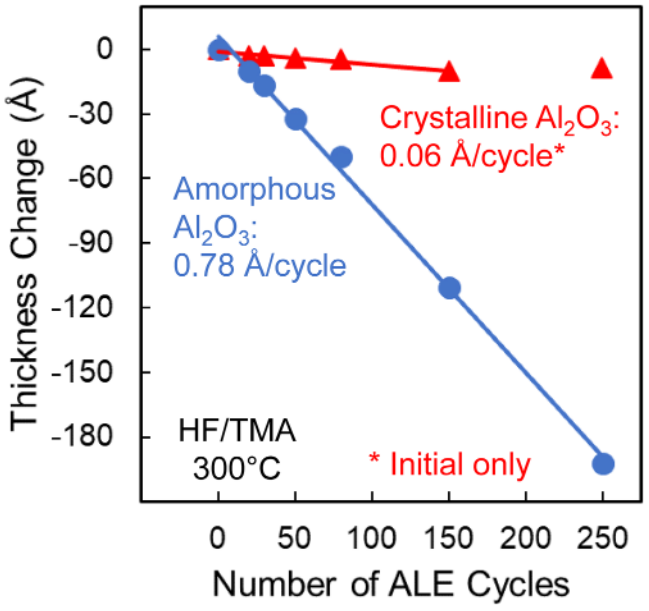

FIG. 4. Thickness change vs number of ALE cycles for amorphous and crystalline Al_2O_3 films using HF and TMA as reactants at 300 °C.

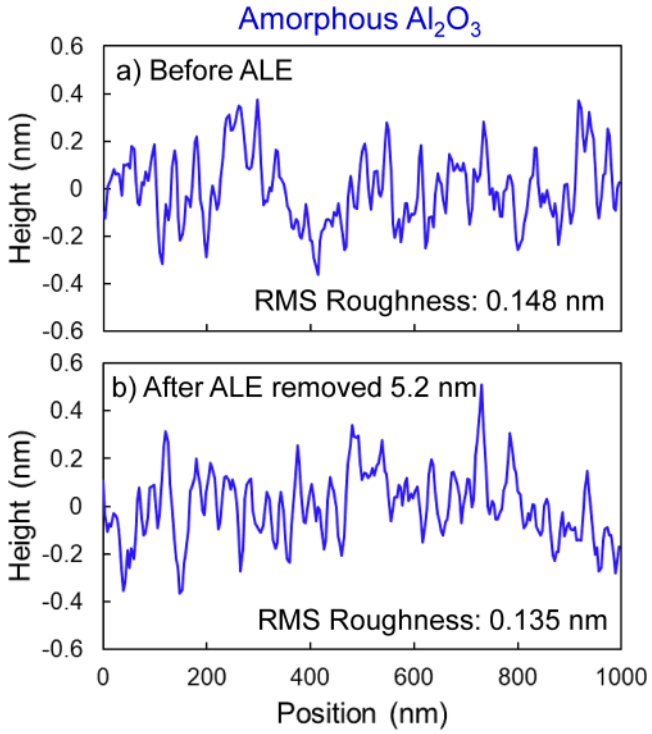

FIG. 5. AFM line scans (a) before and (b) after Al_2O_3 ALE that removed a thickness of 5.2 nm for amorphous Al_2O_3 films at 300 °C using HF and TMA as reactants.

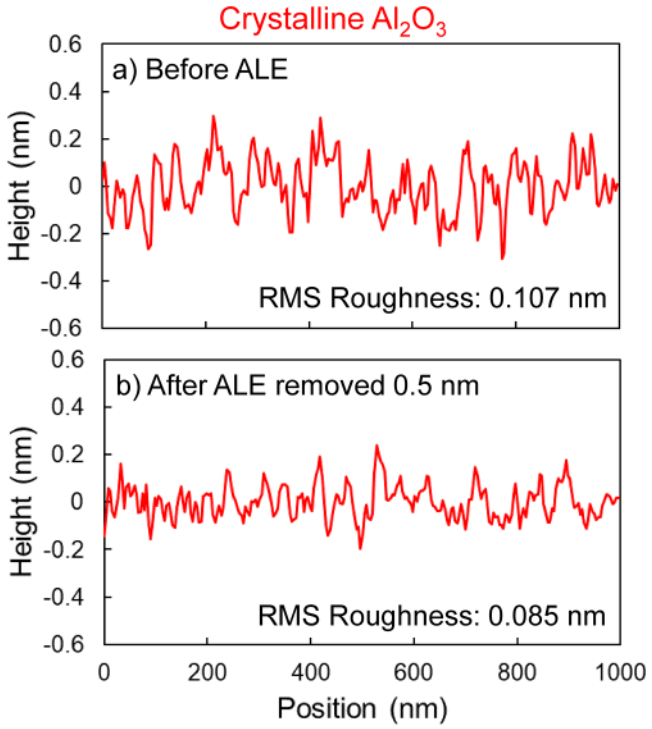

FIG. 6. AFM line scans (a) before and (b) after Al_2O_3 ALE that removed a thickness of 0.5 nm for crystalline Al_2O_3 films at 300 °C using HF and TMA as reactants.

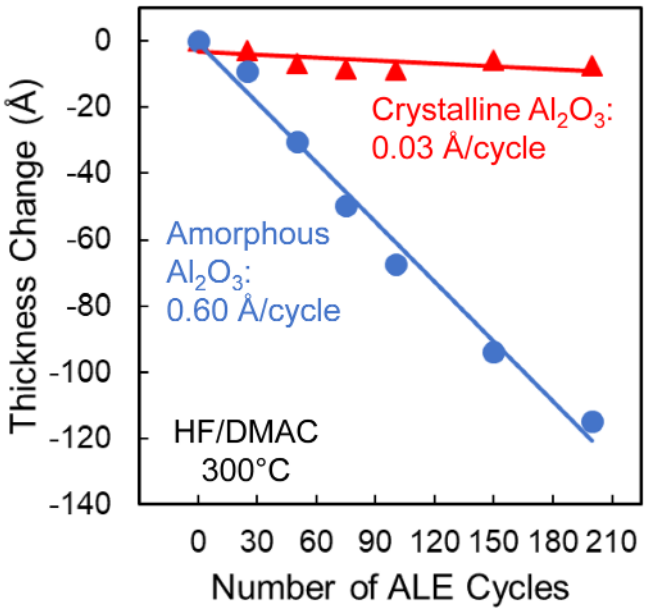

FIG. 7. Thickness change vs number of ALE cycles for amorphous and crystalline Al_2O_3 films using HF and DMAC as reactants at 300 °C.

and possibly higher etch rates at crystalline grain boundaries caused an increase in the surface roughness after Al_2O_3 ALE using HF and TMA as the reactants.

DMAC is also an effective ligand-exchange reactant for the ALE of amorphous Al_2O_3 ALD films.[14,26,27] Figure 7 shows the thermal ALE results using HF and DMAC at 300 °C. The amorphous Al_2O_3 ALD film had an etch rate of 0.60 Å/cycle. This etch rate for the amorphous Al_2O_3 film is comparable to previous results using HF and DMAC as the reactants at 300 °C.[14,26] AFM results indicated that the RMS roughness increased slightly using HF and DMAC as the reactants. The RMS roughness increased from 0.148 nm for the initial amorphous Al_2O_3 film to 0.266 nm after 200 ALE cycles.

In contrast to the amorphous Al_2O_3 film, Fig. 7 reveals that the crystalline Al_2O_3 film had a much lower etch rate of 0.03 Å/cycle using HF and DMAC as the reactants. Similar to the results using HF and TMA as the reactants, the crystalline Al_2O_3 films have a much lower etch rate than the amorphous Al_2O_3 films. AFM results showed that the RMS roughness of the crystalline Al_2O_3 films was nearly equivalent after etching using HF and DMAC as the reactants. For the crystalline Al_2O_3 films, the RMS roughness was 0.107 nm for the initial films and 0.136 nm after 200 ALE cycles.

The ALE of amorphous and crystalline ZrO_2 films was explored earlier using HF and DMAC as the reactants at 250 °C.[28] There was little difference between the amorphous and crystalline ZrO_2 films at 250 °C. The amorphous ZrO_2 films displayed an etch rate of 1.11 Å/cycle.[28] The crystalline ZrO_2 films yielded only a slightly smaller etch rate of 0.82 Å/cycle.[28] The contrast between the etch rates for amorphous and crystalline films of ZrO_2 and Al_2O_3 may be attributed to the larger molar volume expansion upon fluorination for crystalline Al_2O_3. The ratio of molar volumes for $2AlF_3$ and crystalline Al_2O_3 is 2.08. In comparison, the ratio of molar volumes for ZrF_4 and crystalline ZrO_2 is 1.74. The larger expansion upon fluorination of crystalline Al_2O_3 to $2AlF_3$ may inhibit fluorination and restrict the etching of crystalline Al_2O_3 films.

B. Al_2O_3 etching versus annealing temperature using HF and TMA as reactants

The second set of Al_2O_3 samples that had been annealed to 400, 600, 800, and 1000 °C was used to determine how the etch rate changes as the Al_2O_3 films become more crystalline. Figure 8 shows the results for Al_2O_3 ALE using HF and TMA as the reactants at 300 °C. These results include the as-deposited Al_2O_3 ALD film. The as-deposited Al_2O_3 film, as well as the Al_2O_3 films annealed to 400, 600, and 800 °C all had an etch rate of 0.78 Å/cycle. In contrast, the Al_2O_3 film annealed to 1000 °C displayed a much lower etch rate of 0.09 Å/cycle.

These etching results correlate well with the GI-XRD results for these same samples shown in Fig. 2. The films annealed up to 800 °C do not display crystallinity as measured by GI-XRD and have nearly the same etch rate. The Al_2O_3 film annealed at 1000 °C was the only crystalline film and yielded a much lower etch rate. The results in Fig. 2 indicate that the crystallization of the

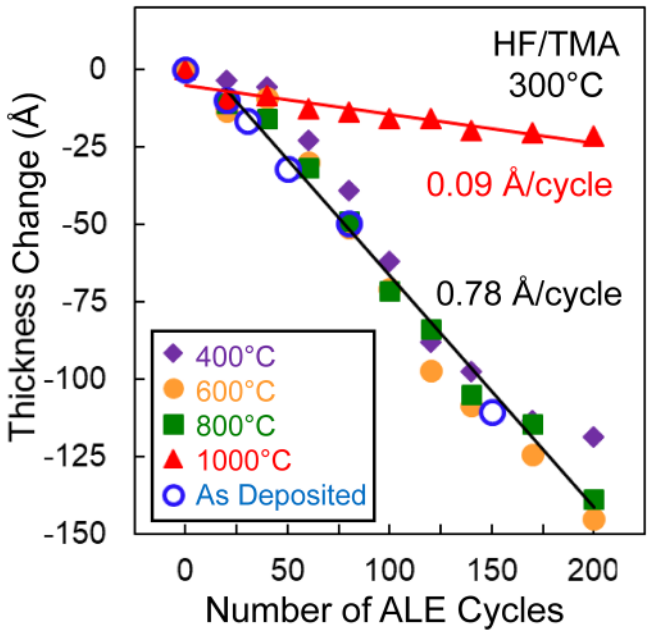

FIG. 8. Thickness change vs number of ALE cycles for Al_2O_3 films annealed at 400–1000 °C using HF and TMA as reactants at 300 °C.

amorphous Al_2O_3 ALD films occurs between 800 and 1000 °C. To probe annealing temperatures between 800 and 1000 °C, amorphous Al_2O_3 ALD films were annealed in increments of 40 °C between 800 and 1000 °C. This defined the third set of samples.

Figure 9 shows the Al_2O_3 ALE results at 300 °C for the amorphous Al_2O_3 ALD films annealed between 800 and 1000 °C.

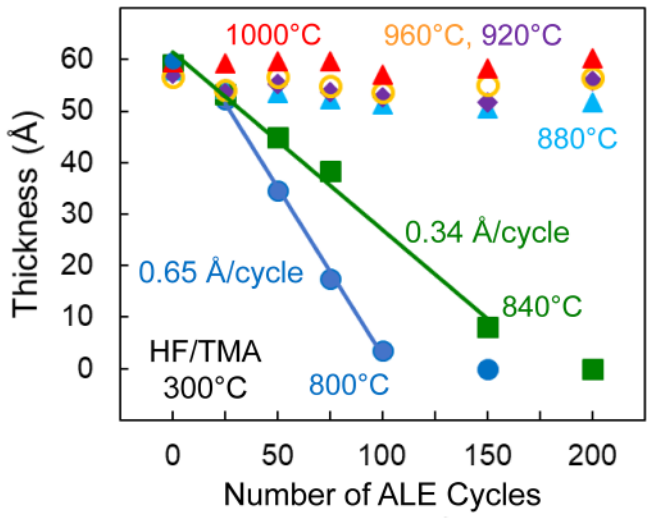

FIG. 9. Thickness change vs number of ALE cycles for Al_2O_3 films annealed at 800–1000 °C using HF and TMA as reactants at 300 °C.

The Al_2O_3 ALE was conducted using HF and TMA as the reactants. The Al_2O_3 films annealed at 800 °C had an etch rate of 0.65 Å/cycle. This etch rate of 0.65 Å/cycle for Al_2O_3 films from the third set of samples annealed at 800 °C is slightly less than the etch rate of 0.78 Å/cycle observed in Fig. 8 for Al_2O_3 films from the second set of samples annealed at 800 °C. This variation is attributed to the different Al_2O_3 ALD conditions employed for the second and third set of Al_2O_3 samples.

Figure 9 also reveals that the Al_2O_3 films annealed at 840 °C had a slower etch rate of 0.34 Å/cycle. This result suggests that the Al_2O_3 films annealed at 840 °C are partially crystalline. In contrast, the films annealed at 880 °C or higher temperatures had a negligible etch rate. Based on these Al_2O_3 ALE results, the Al_2O_3 films may be fully crystalline at annealing temperatures of 880 °C and above.

This suggestion can be tested using diffraction studies to determine the crystallinity of the Al_2O_3 ALD films. GI-XRD scans of the amorphous Al_2O_3 ALD films annealed between 800 and 1000 °C are displayed in Fig. 10. The Al_2O_3 films annealed at 880–1000 °C all display crystallinity with a diffraction peak at 67° that is expected for gamma-Al_2O_3 or delta-Al_2O_3 (Refs. 34 and 42). The peak intensities are lower for these GI-XRD scans compared with the GI-XRD scans shown in Fig. 2 because the film thicknesses were smaller at approximately 5 nm.

The Al_2O_3 film annealed to 800 °C does not display a diffraction peak. The Al_2O_3 film annealed at 840 °C displayed a reduced etch rate of 0.34 Å/cycle in Fig. 9. However, the Al_2O_3 film annealed at 840 °C does not appear crystalline by the GI-XRD scan. The threshold for the film crystallinity as measured by GI-XRD is reached for the Al_2O_3 film annealed at 880 °C.

There are dramatic differences between the ALE of amorphous and crystalline Al_2O_3 films. Figure 3 shows that the amorphous Al_2O_3 film has a lower density of approximately 3.0 g/cm^3 compared with the higher density of 3.63 g/cm^3 for the crystalline Al_2O_3 film. The lower density may facilitate fluorination because fluorination leads to expansion of the metal oxide.

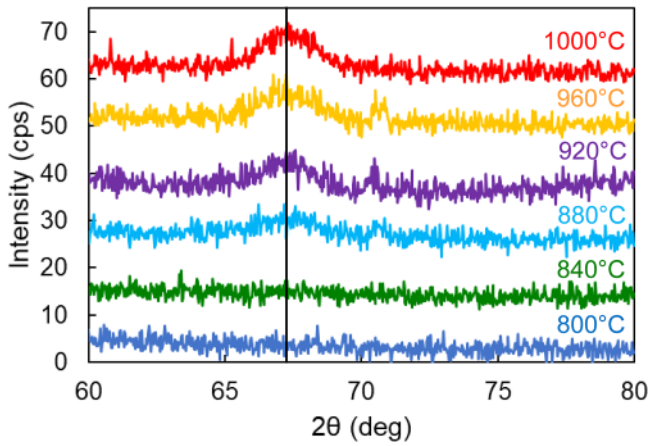

FIG. 10. GI-XRD scans for amorphous Al_2O_3 films annealed to 800, 840, 880, 920, 960, and 1000 °C. The prominent peak at 67° is consistent with gamma-Al_2O_3 or delta-Al_2O_3.

For example, for crystalline gamma-Al_2O_3, the molar volume is 101.96 g/mol/3.63 g/cm^3 = 28.088 cm^3/mol. In contrast, the molar volume of crystalline AlF_3 is 83.98 g/mol/2.88 g/cm^3 = 29.160 cm^3/mol. The volume expansion upon fluorination of crystalline Al_2O_3 to $2AlF_3$ is 2.08.

Molecular dynamics simulations have also examined the structure of amorphous and gamma-Al_2O_3.[44] These studies indicate that the surfaces of amorphous and gamma-Al_2O_3 are very similar. First principles calculations also point out the similarity between $(Al_2O_3)_m$ clusters and gamma-Al_2O_3.[45] Therefore, the surfaces on amorphous and gamma-Al_2O_3 would not be expected to lead to differences in the etch rates. However, the simulations confirm the higher density of gamma-Al_2O_3 compared with amorphous Al_2O_3.[44] The computations also can examine the coordination number and ring distribution in amorphous and gamma-Al_2O_3. An n-fold ring is defined as the shortest path of alternating Al–O bonds and an n-fold ring consists of 2n alternating Al–O bonds.[44] The coordination number and ring distribution change between amorphous Al_2O_3 and gamma-Al_2O_3.

Amorphous Al_2O_3 has a dominant Al coordination number of 4 and a ring distribution of mostly fourfold rings.[44] Amorphous Al_2O_3 is also largely composed of AlO_4 polyhedra. In contrast, gamma-Al_2O_3 has a dominant Al coordination number of 6 and a ring distribution of mostly twofold and threefold rings.[44] Gamma-Al_2O_3 is also largely composed of AlO_6 polyhedra. The etching of Al_2O_3 may be more difficult for the more highly coordinated Al centers in gamma-Al_2O_3. These highly coordinated Al centers may be less accessible for the fluorination reaction. Thinner fluoride layers on Al_2O_3 during Al_2O_3 ALE have earlier been shown to lead to smaller etch rates.[9]

A previous study investigated the thermodynamics of HF fluorination of Al_2O_3.[10] This study found that desorption of water was the step with the highest energy barrier during HF fluorination.[10] The denser structure of crystalline gamma-Al_2O_3 compared with amorphous Al_2O_3 may also inhibit the desorption of water and reduce the HF fluorination of Al_2O_3.

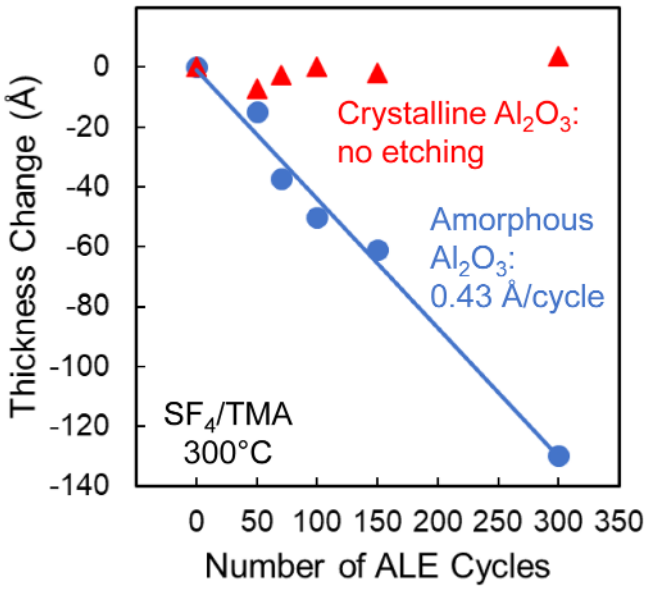

FIG. 11. Thickness change vs number of ALE cycles for amorphous and crystalline Al_2O_3 films using SF_4 and TMA as reactants at 300 °C.

C. Al_2O_3 etching with SF_4 or XeF_2 as fluorination reactant

Other fluorination agents can be utilized in place of HF during thermal ALE. For example, SF_4 is another possible fluorinating agent that has been previously used in thermal ALE.[46] SF_4 is known to be a stronger fluorination agent for metal oxides. The standard free energy changes during fluorination of Al_2O_3 to AlF_3 using HF or SF_4 illustrate this difference,[47]

$$Al_2O_3 + 6HF(g) \rightarrow 2AlF_3 + 3H_2O(g),\ \Delta G^\circ(300\,^\circ C) = -49.0\,\text{kcal}, \quad (1)$$

$$Al_2O_3 + 3/2SF_4(g) \rightarrow 2AlF_3 + 3/2SO_2(g),\ \Delta G^\circ(300\,^\circ C) = -155.9\,\text{kcal}. \quad (2)$$

A more favorable fluorination reaction could result in a thicker fluoride layer. The ligand-exchange reaction could then remove more of the fluoride layer and yield a higher etch rate.

Thermal ALE using SF_4 and TMA as the reactants at 300 °C is shown in Fig. 11. Amorphous Al_2O_3 has an etch rate of 0.43 Å/cycle. In contrast, crystalline Al_2O_3 does not display any etching. The etch rate for amorphous Al_2O_3 is also lower with SF_4 than with HF. The etch rates for amorphous Al_2O_3 using HF or SF_4 and TMA as the reactants are 0.78 or 0.43 Å/cycle, respectively. The etch rates are not correlating with the standard free energy changes for fluorination. The use of SF_4 as the fluorination reactant also led to an increase in the RMS roughness. The RMS roughness increased from 0.148 nm for the initial amorphous Al_2O_3 film to 0.624 nm after 150 ALE cycles using SF_4 and TMA. Although there was no measurable etching of the crystalline Al_2O_3 film using SF_4 and TMA, the crystalline Al_2O_3 film increased in RMS roughness to 0.502 nm after 150 ALE cycles.

Earlier etch rates for Al_2O_3 using $Sn(acac)_2$ as the ligand-exchange reactant and either HF or SF_4 as the fluorination reactant also did not scale with the standard free energy changes for fluorination. The etch rate for amorphous Al_2O_3 using HF or

SF_4 and $Sn(acac)_2$ as the reactants at 200 °C were 0.28 or 0.20 Å/cycle, respectively.[4,12,46] Perhaps there are additional kinetic factors that favor fluorination using HF. For example, H_2O is the product of HF fluorination of Al_2O_3.[10] In contrast, SF_4 is postulated to release SO_2 according to Eq. (2). Another possible sulfur-containing etch product is SOF_2.[46] The kinetic pathways leading to SO_2 or SOF_2 desorption may be more difficult than the kinetic pathways leading to H_2O desorption. These kinetic bottlenecks may reduce the etch rate using SF_4 as the fluorination reactant.

Another possible fluorination agent for thermal ALE is XeF_2.[18] XeF_2 has an even larger standard free energy change for fluorination of Al_2O_3 than HF or SF_4,[47]

$$Al_2O_3 + 3XeF_2(g) \rightarrow 2AlF_3 + 3/2O_2(g) + 3Xe(g), \Delta G^\circ(300\,^\circ C) = -266.5\,\text{kcal}. \quad (3)$$

Figure 12 shows the results for Al_2O_3 ALE using XeF_2 and TMA as the reactants at 300 °C. The etch rate for amorphous Al_2O_3 is 0.66 Å/cycle. This etch rate using XeF_2 is slightly less than the etch rate of 0.78 Å/cycle for amorphous Al_2O_3 using HF and TMA as the reactants from Fig. 4. The etch rate using XeF_2 is also somewhat larger than the etch rate of 0.43 Å/cycle for amorphous Al_2O_3 using SF_4 and TMA as the reactants from Fig. 11. These results again do not argue that the Al_2O_3 etch rate is proportional to the standard free energy changes for Al_2O_3 fluorination. Using XeF_2 as the fluorination reactant did not increase the RMS roughness for the amorphous Al_2O_3 films. The RMS roughness was 0.148 nm for the initial amorphous Al_2O_3 film and nearly equivalent at 0.133 nm after 50 ALE cycles using XeF_2 and TMA as the reactants.

Figure 12 also shows results for the etching of crystalline Al_2O_3 using XeF_2 and TMA as the reactants at 300 °C. These crystalline samples were annealed to 1000 °C. There is evidence that etching of the crystalline Al_2O_3 proceeds for about 17 Å before the etching stops. Similar behavior was observed for etching crystalline Al_2O_3 with HF and TMA as the reactants in Fig. 4. This behavior suggests that the bulk crystalline Al_2O_3 does not etch. However, a modified or damaged surface of the crystalline Al_2O_3 film may be accessible to etching. This idea is supported by the large increase in RMS roughness observed after 50 ALE cycles using XeF_2 and TMA as the reactants. The RMS roughness increased from 0.107 nm for the initial crystalline Al_2O_3 film to 7.923 nm after 50 ALE cycles using XeF_2 and TMA.

Etching experiments were also performed with XeF_2 and DMAC as the ligand-exchange reactant at 300 °C. Figure 13 shows that the etch rate for amorphous Al_2O_3 is 0.81 Å/cycle. This etch rate using XeF_2 is slightly larger than the etch rate of 0.78 Å/cycle for amorphous Al_2O_3 using HF and TMA as the reactants from Fig. 4.

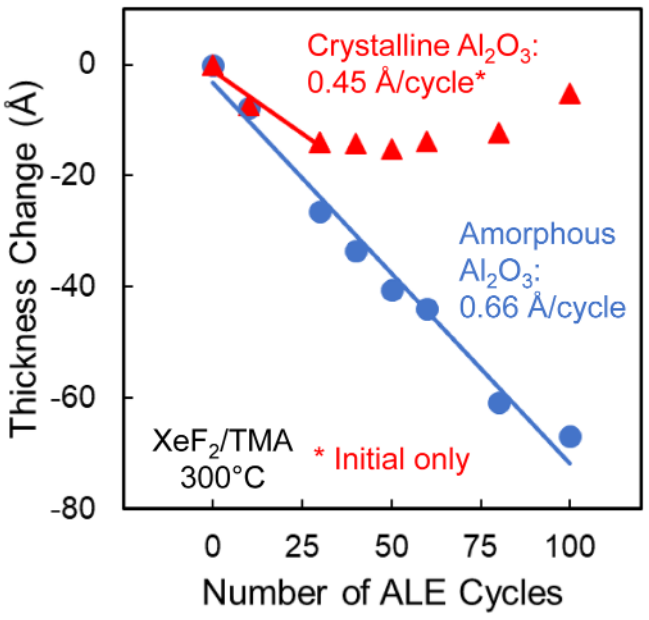

FIG. 12. Thickness change vs number of ALE cycles for amorphous and crystalline Al_2O_3 films using XeF_2 and TMA as reactants at 300 °C.

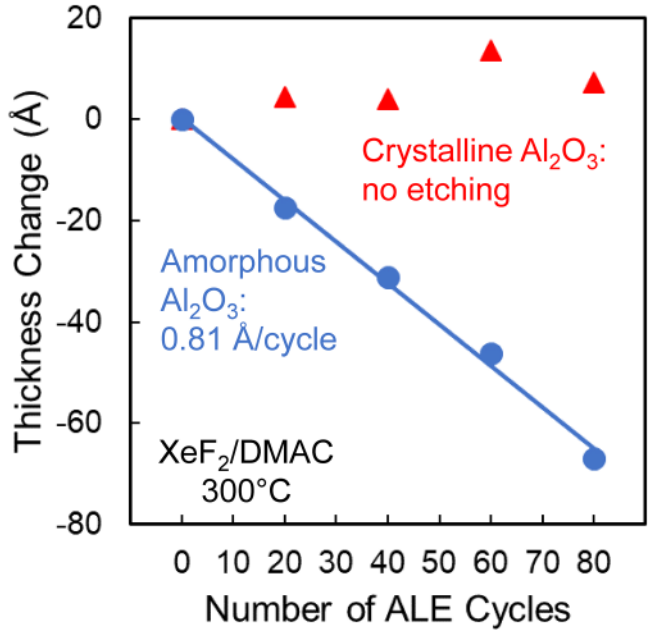

FIG. 13. Thickness change vs number of ALE cycles for amorphous and crystalline Al_2O_3 films using XeF_2 and DMAC as reactants at 300 °C.

TABLE I. Etch rates using different fluorination reactants and metal precursors for ligand-exchange at 300 °C for amorphous and crystalline Al_2O_3 films.

Fluorination reactant	Ligand-exchange reactant	Amorphous Al_2O_3 (Å/cycle)	Crystalline Al_2O_3 (Å/cycle)
HF	TMA	0.78	0.06[a]
HF	DMAC	0.60	0.03
SF_4	TMA	0.43	No etch
XeF_2	TMA	0.66	0.45[a]
XeF_2	DMAC	0.81	No etch

[a]Initial etching only before etching stops.

The etch rate using XeF_2 and DMAC is also somewhat larger than the etch rate of 0.66 Å/cycle for amorphous Al_2O_3 using XeF_2 and TMA as the reactants from Fig. 12. AFM measurements also revealed that the RMS surface roughness increased after Al_2O_3 ALE using XeF_2 and DMAC. The RMS roughness increased from 0.148 nm for the initial amorphous Al_2O_3 film to 0.832 nm after 150 ALE cycles. A summary of all the Al_2O_3 etch rates for amorphous Al_2O_3 at 300 °C is given in Table I.

Figure 13 also indicates that the crystalline Al_2O_3 does not etch with XeF_2 and DMAC at 300 °C. In fact, there may be a slight deposition on the Al_2O_3 surface under these conditions. The RMS roughness also increased to 0.613 nm after 80 cycles resulting from the XeF_2 and DMAC exposures on crystalline Al_2O_3. Earlier experiments have monitored the deposition of AlF_3 on Al_2O_3 using HF and TMA at much lower temperatures.[48,49] The lack of etching in Fig. 13 is consistent with all the previous experiments on crystalline Al_2O_3. A summary of all the Al_2O_3 etch rates for crystalline Al_2O_3 at 300 °C is provided in Table I. Either there is no etching of crystalline Al_2O_3 or there is a slight amount of etching before the etching stops after removing 10–17 Å of the top surface layer.

XeF_2 has been shown to spontaneously etch silicon.[50] A proximity effect also resulted in the spontaneous etching of SiO_2 by XeF_2 in the presence of Si.[51] To determine if XeF_2 alone could spontaneously etch Al_2O_3, both the crystalline and amorphous Al_2O_3 samples were subjected to 100 exposures of XeF_2 at 300 °C. Each XeF_2 exposure was conducted for 3 s followed by a purge of 30 s. After 25 XeF_2 exposures, there was a small thickness loss of 5 Å or less of the top surface layer on each sample. Further XeF_2 exposures beyond 25 exposures showed no thickness change for either sample. These control experiments rule out the spontaneous etching of amorphous Al_2O_3 at 300 °C. Only a small fraction of the 10–17 Å removed from crystalline Al_2O_3 prior to the stoppage of etching could be accounted for by spontaneous etching of Al_2O_3 by XeF_2.

IV. CONCLUSIONS

The thermal ALE for amorphous and crystalline Al_2O_3 films was compared at 300 °C using HF, SF_4, or XeF_2 as the fluorination reactants and TMA or DMAC as the metal precursors for ligand-exchange. The etch rates for the amorphous films were much higher than the etch rates for the crystalline films. For example, the etch rate for amorphous Al_2O_3 prior to any annealing using HF and TMA as the reactants was 0.78 Å/cycle. In comparison, the etch rate for crystalline Al_2O_3 formed by annealing at 1000 °C using HF and TMA as the reactants was approximately 0.06 Å/cycle for the first 10 Å and then negligible for larger Al_2O_3 thicknesses. The RMS surface roughness of both the amorphous and crystalline Al_2O_3 films was slightly reduced by thermal Al_2O_3 ALE using HF and TMA as the reactants.

Etch rates were measured at 300 °C using the following pairs of fluorination/ligand-exchange reactants: HF/TMA; HF/DMAC; SF_4/TMA; XeF_2/TMA; and XeF_2/DMAC. HF/TMA and XeF_2/DMAC resulted in the highest etch rates for amorphous Al_2O_3 prior to any annealing of approximately 0.8 Å/cycle. XeF_2/TMA and HF/DMAC etch rates for amorphous Al_2O_3 were comparable at around 0.6 Å/cycle. The SF_4/TMA etch rate for amorphous Al_2O_3 was the lowest at around 0.4 Å/cycle. Etching the amorphous Al_2O_3 with XeF_2/TMA and SF_4/TMA led to higher RMS surface roughness. In comparison, the etch rates for crystalline Al_2O_3 after annealing to 1000 °C using the same pairs of fluorination/ligand-exchange reactants were much smaller or negligible. However, the RMS surface roughness of the crystalline Al_2O_3 film was noticeably larger after exposures to XeF_2/TMA, XeF_2/DMAC, and SF_4/TMA.

The Al_2O_3 crystallinity and etch rates were also investigated versus anneal temperature. The amorphous Al_2O_3 film remains amorphous for annealing temperatures up to 800 °C. These amorphous Al_2O_3 films also displayed a constant etch rate of 0.78 Å/cycle using the HF and TMA reactants at 300 °C. Crystallinity in Al_2O_3 films starts to appear after annealing at 880 °C. In comparison, the etch rate of the amorphous Al_2O_3 films using the HF and TMA reactants is reduced to 0.34 Å/cycle after annealing at 840 °C. All the films annealed to 880 °C and higher temperatures displayed the same negligible etch rate using HF and TMA as the reactants. In comparison, the intensity of the diffraction peak increases progressively for temperatures higher than 880 °C.

The differences between the etch rates of amorphous and crystalline Al_2O_3 films can be attributed to their different densities. Amorphous materials have a lower density than their crystalline counterparts. The lower density may facilitate fluorination because fluorination leads to a significant molar volume expansion. The lower density and lower coordination of Al centers in amorphous Al_2O_3 may also allow for an easier replacement of oxygen with fluorine during fluorination. A larger fluoride film thickness after fluorination can lead to more fluoride removed during the ligand-exchange reaction and larger etch rates.

The etch rates of Al_2O_3 by the HF, SF_4, and XeF_2 fluorination reactants together with either TMA or DMAC as the ligand-exchange precursor did not correspond with their standard free energy changes for Al_2O_3 fluorination. This lack of correlation suggests that kinetic factors must also be important during Al_2O_3 fluorination. In addition, the difference between the etch rates for amorphous and crystalline Al_2O_3 indicates that amorphous Al_2O_3 could easily be etched in the presence of crystalline Al_2O_3. This structure dependent etching selectivity could be used to remove amorphous Al_2O_3 while retaining crystalline Al_2O_3.

ACKNOWLEDGMENTS

This research was funded by the National Science Foundation (NSF) (No. CHE-1609554).

DATA AVAILABILITY

The data that support the findings of this study are available within the article.

REFERENCES

[1]K. J. Kanarik, T. Lill, E. A. Hudson, S. Sriraman, S. Tan, J. Marks, V. Vahedi, and R. A. Gottscho, J. Vac. Sci. Technol. A **33**, 020802 (2015).
[2]G. S. Oehrlein, D. Metzler, and C. Li, ECS J. Solid State Sci. Technol. **4**, N5041 (2015).
[3]S. M. George, Acc. Chem. Res. **53**, 1151 (2020).
[4]Y. Lee and S. M. George, ACS Nano **9**, 2061 (2015).
[5]C. T. Carver, J. J. Plombon, P. E. Romero, S. Suri, T. A. Tronic, and R. B. Turkot, ECS J. Solid State Sci. Technol. **4**, N5005 (2015).
[6]T. Faraz, F. Roozeboom, H. C. M. Knoops, and W. M. M. Kessels, ECS J. Solid State Sci. Technol. **4**, N5023 (2015).
[7]S. M. George, Chem. Rev. **110**, 111 (2010).
[8]S. M. George and Y. Lee, ACS Nano **10**, 4889 (2016).
[9]A. M. Cano, A. E. Marquardt, J. W. DuMont, and S. M. George, J. Phys. Chem. C **123**, 10346 (2019).
[10]S. K. Natarajan and S. D. Elliott, Chem. Mater. **30**, 5912 (2018).
[11]J. W. Clancey, A. S. Cavanagh, J. E. T. Smith, S. Sharma, and S. M. George, J. Phys. Chem. C **124**, 287 (2020).
[12]Y. Lee, J. W. DuMont, and S. M. George, Chem. Mater. **27**, 3648 (2015).
[13]Y. Lee, J. W. DuMont, and S. M. George, Chem. Mater. **28**, 2994 (2016).
[14]Y. Lee, C. Huffman, and S. M. George, Chem. Mater. **28**, 7657 (2016).
[15]Y. Lee and S. M. George, J. Vac. Sci. Technol. A **36**, 061504 (2018).
[16]Y. Lee, N. R. Johnson, and S. M. George, Chem. Mater. **32**, 5937 (2020).
[17]N. R. Johnson, H. Sun, K. Sharma, and S. M. George, J. Vac. Sci. Technol. A **34**, 050603 (2016).
[18]N. R. Johnson, J. K. Hite, M. A. Mastro, C. R. Eddy, and S. M. George, Appl. Phys. Lett. **114**, 243103 (2019).
[19]T. J. Myers, A. M. Cano, D. K. Lancaster, J. W. Clancey, and S. M. George, J. Vac. Sci. Technol. A **39**, 021001 (2021).
[20]J. W. DuMont, A. E. Marquardt, A. M. Cano, and S. M. George, ACS Appl. Mater. Interfaces **9**, 10296 (2017).
[21]D. R. Zywotko and S. M. George, Chem. Mater. **29**, 1183 (2017).
[22]N. R. Johnson and S. M. George, ACS Appl. Mater. Interfaces **9**, 34435 (2017).
[23]A. I. Abdulagatov and S. M. George, Chem. Mater. **30**, 8465 (2018).
[24]A. I. Abdulagatov and S. M. George, J. Vac. Sci. Technol. A **38**, 022607 (2020).
[25]A. I. Abdulagatov, V. Sharma, J. A. Murdzek, A. S. Cavanagh, and S. M. George, J. Vac. Sci. Technol. A **39**, 022602 (2021).
[26]Y. Lee and S. M. George, J. Phys. Chem. C **123**, 18455 (2019).
[27]A. Fischer, A. Routzahn, Y. Lee, T. Lill, and S. M. George, J. Vac. Sci. Technol. A **38**, 022603 (2020).
[28]J. A. Murdzek and S. M. George, J. Vac. Sci. Technol. A **38**, 022608 (2020).
[29]I. Levin and D. Brandon, J. Am. Ceram. Soc. **81**, 1995 (1998).
[30]S. K. Lee, S. B. Lee, S. Y. Park, Y. S. Yi, and C. W. Ahn, Phys. Rev. Lett. **103**, 095501 (2009).
[31]S. K. Lee, S. Y. Park, Y. S. Yi, and J. Moon, J. Phys. Chem. C **114**, 13890 (2010).
[32]P. Nayar, A. Khanna, D. Kabiraj, S. R. Abhilash, B. D. Beake, Y. Losset, and B. Chen, Thin Solid Films **568**, 19 (2014).
[33]Z. Hsain, G. Zeng, N. C. Strandwitz, and B. A. Krick, Wear **372–373**, 139 (2017).
[34]S. Jakschik, U. Schroeder, T. Hecht, M. Gutsche, H. Seidl, and J. W. Bartha, Thin Solid Films **425**, 216 (2003).
[35]G. Krautheim, T. Hecht, S. Jakschik, U. Schröder, and W. Zahn, Appl. Surf. Sci. **252**, 200 (2005).
[36]L. Bloch, Y. Kauffmann, and B. Pokroy, Cryst. Growth Des. **14**, 3983 (2014).
[37]E. P. Gusev, C. Cabral, M. Copel, C. D'Emic, and M. Gribelyuk, Microelectron. Eng. **69**, 145 (2003).
[38]L. Zhang, J. Zhang, H. Jiao, G. Bao, Z. Wang, and X. Cheng, Thin Solid Films **642**, 359 (2017).
[39]G. Pant, A. Gnade, M. J. Kim, R. M. Wallace, B. E. Gnade, M. A. Quevedo-Lopez, and P. D. Kirsch, Appl. Phys. Lett. **88**, 032901 (2006).
[40]E. Yurchuk, J. Müller, S. Knebel, J. Sundqvist, A. P. Graham, T. Melde, U. Schröder, and T. Mikolajick, Thin Solid Films **533**, 88 (2013).
[41]J. W. Elam, M. D. Groner, and S. M. George, Rev. Sci. Instrum. **73**, 2981 (2002).
[42]S. R. Chauruka, A. Hassanpour, R. Brydson, K. J. Roberts, M. Ghadiri, and H. Stitt, Chem. Eng. Sci. **134**, 774 (2015).
[43]M. D. Groner, F. H. Fabreguette, J. W. Elam, and S. M. George, Chem. Mater. **16**, 639 (2004).
[44]G. Gutiérrez and B. Johansson, Phys. Rev. B **65**, 104202 (2002).
[45]A. B. Rahane, M. D. Deshpande, and V. Kumar, J. Phys. Chem. C **115**, 18111 (2011).
[46]J. C. Gertsch, A. M. Cano, V. M. Bright, and S. M. George, Chem. Mater. **31**, 3624 (2019).
[47]HSC Chemistry, HSC Chemistry 9.9, Outokumpu Research Oy, Pori, Finland.
[48]Y. Lee, J. W. DuMont, A. S. Cavanagh, and S. M. George, J. Phys. Chem. C **119**, 14185 (2015).
[49]Y. Lee, H. X. Sun, M. J. Young, and S. M. George, Chem. Mater. **28**, 2022 (2016).
[50]H. F. Winters and J. W. Coburn, Appl. Phys. Lett. **34**, 70 (1979).
[51]J. F. Veyan, M. D. Halls, S. Rangan, D. Aureau, X. M. Yan, and Y. J. Chabal, J. Appl. Phys. **108**, 114914 (2010).